

Isospin Effect on the Process of Multifragmentation and Dissipation at Intermediate Energy Heavy Ion Collisions

Jian-Ye Liu^{1,2,3}, Yan-Fang Yang³, Wei Zuo^{1,2,3}
Shun-Jin Wang^{1,2,4}, Qiang Zhao³, Wen-Jun Guo³, Bo Chen³

¹CCAST (World Lab.), P.O.Box 8730, Beijing 100080

²Center of Theoretical Nuclear Physics, National Laboratory of Heavy Ion Accelerator
Lanzhou 730000, P. R. China

³Institute of Modern Physics, Chinese Academy of Sciences, P. O. Box 31
Lanzhou 730000, P. R. China

⁴Institute of Modern Physics, southwest Jiaotong University, Chendu 610031, P. R. China

Abstract

In the simulation of intermediate energy heavy ion collisions by using the isospin dependent quantum molecular dynamics, the isospin effect on the process of multifragmentation and dissipation has been studied. It is found that the multiplicity of intermediate mass fragments N_{imf} for the neutron-poor colliding system is always larger than that for the neutron-rich system, while the quadrupole of single particle momentum distribution Q_{zz} for the neutron-poor colliding system is smaller than that of the neutron-rich system for all projectile-target combinations studied at the beam energies from about 50MeV/nucleon to 150MeV/nucleon. Since Q_{zz} depends strongly on isospin dependence of in-medium nucleon-nucleon cross section and weakly on symmetry potential at the above beam energies, it may serve as a good probe to extract the information on the in-medium nucleon-nucleon cross section. The correlation between the multiplicity N_{imf} of intermediate mass fragments and the total number of charged particles N_c has the behavior similar to Q_{zz} , which can be used as a complementary probe to the in-medium nucleon-nucleon cross section.

PACs Number(s): 25.70.pg, 02.70.Ns, 24.10.Lx

Keywords: isospin effect, multifragmentation, dissipation, nucleon-nucleon cross section

1 Introduction

In recent years, the establishment of radioactive beam facilities at many laboratories over the world and the use of radioactive beams with large neutron or proton excess have offered an excellent opportunity to investigate the isospin-dependence of heavy ion collision (HIC) dynamics^[1-4]. This kind of study has made it possible to obtain the information about the equation of state (EOS) of asymmetric nuclear matter ranging from symmetric nuclear matter to pure neutron matter and the information on isospin-dependence of in-medium nucleon-nucleon (N-N) cross section, which are significantly important not only in understanding nuclear properties but also in exploring the explosion mechanism of supernova and the cooling rate of neutron stars. However two essential ingredients in HIC dynamics, the symmetry potential of the mean field and the isospin-dependent in-medium N-N cross section, have not been well determined so far. Recently, Li et al.^[1,5,6] made use of the isospin dependent transport theory to investigate nuclear symmetry energy and showed that the rate of pre-equilibrium neutron-proton emitted in intermediate energy HIC is sensitive to the density dependence of nuclear symmetry potential, but insensitive to the incompressibility of symmetric nuclear matter and the in-medium N-N cross section. Also, R.Pak and Bao-An Li et al. have found that the isospin dependence of collective flow and balance energy are mainly originated from the isospin-dependent in-medium N-N cross section^{[5],[7-11]}. Recently we have found that nuclear stopping can be used as a good probe for exploring the in-medium N-N cross section in HIC in the beam energy ranging from above Fermi energy to 150MeV/nucleon. However, it is still not clear how the nuclear stopping depends on the neutron-proton ratio of the colliding system^[12]. In viewing that little information is known about the in-medium N-N cross section and its isospin dependence up to now, it is thus very desirable to find an efficient way to gain such kind of knowledge.

It is known that many intermediate mass fragments(IMF) are emitted in the process of intermediate energy HIC and that the element distribution and fragment multiplicity indicate a strong correlation between the multiplicity of intermediate mass fragments

N_{imf} and the total number of charged particles N_c [7]. The question is whether the multifragmentation and dissipation, especially the N_{imf} and Q_{zz} are sensitive to the neutron-proton ratio of the colliding system. To answer this question, we have investigated the isospin effect on the process of multifragmentation and dissipation in HIC for the colliding systems with different ratios of neutron to proton by using isospin dependent quantum molecular dynamics (IQMD). To increase the efficiency of detectors and the statistics of N_{imf} and Q_{zz} , the reversible kinetic reactions with heavy projectiles on light targets are suggested to have more intermediate mass fragments emitted towards forward angles.

The calculated results show prominent isospin effect for the multifragmentation N_{imf} and the quadrupole of single particle momentum distribution Q_{zz} for the colliding systems with different neutron or proton excesses. The multiplicity of intermediate mass fragments N_{imf} of neutron-poor systems is always larger than that of neutron-rich systems, while the quadrupole of single particle momentum distribution Q_{zz} for neutron-poor systems is smaller than that of neutron-rich systems at the beam energies from 50MeV/nucleon to 150MeV/nucleon for all the reversible colliding systems studied here. The mechanism responsible for the above isospin effect can be found from the fact that the mean N-N cross section for a neutron-poor system is larger than that of the corresponding neutron-rich system with the same masses of projectile and target. The calculated results also show that the correlation between the multiplicity of intermediate mass fragments N_{imf} and the total number of charged particles N_c , depends strongly on the isospin dependence of in-medium N-N cross section and weakly on the symmetry potential in the chosen beam energy region. In Ref.[12], it is found that Q_{zz} is very sensitive to the isospin dependence of in-medium N-N cross section and insensitive to the symmetry potential. In the present paper, the calculations show that the conclusion drawn in Ref.[12] about Q_{zz} remains true for the reversible kinetic reactions with heavy projectiles on light targets, but it is found that Q_{zz} increases slightly as increasing the neutron-proton ratio of the colliding system. Therefore, Q_{zz} can be a good probe for extracting information on in-medium N-N cross section in HIC

in the beam energies ranging from above Fermi energy to 150MeV/nucleon^[12], while the correlation between N_{imf} and N_c may serve as a complementary one.

2 Theoretical Model

The dynamics of intermediate energy HIC described by QMD^[13–14] contains three ingredients: density dependent mean field, in-medium N-N cross section and Pauli blocking. To describe isospin effect appropriately, QMD should be modified properly: the density dependent mean field should contain correct isospin terms including symmetry energy and Coulomb potential, the in-medium N-N cross section should be different for neutron-neutron (proton-proton) and neutron-proton collisions, and the Pauli blocking should be counted by distinguishing neutrons and protons. In addition, the initial condition of the ground state of two colliding nuclei should also contain isospin information. In the present calculation, the ground state of each colliding nucleus is prepared by using the initial code of IQMD, according to its density distribution obtained from the Skyrme-Hartree-Fock calculation with the parameter set of SKM*^[15]. The interaction potential is as follows,

$$U(\rho) = U^{Sky} + V_c(1 - \tau_z) + U^{sym} + V^{yuk} + U^{MDI} + U^{Pauli} \quad (1)$$

U^{Sky} is the density-dependent Skyrme potential,

$$U^{Sky} = \alpha\left(\frac{\rho}{\rho_0}\right) + \beta\left(\frac{\rho}{\rho_0}\right)^\gamma \quad (2)$$

V_c is Coulomb potential. U^{Yuk} is the Yukawa potential^[13],

$$U_j^{Yuk} = t_3 \sum_{i \neq j} \frac{e^{L/m^2}}{r_{ij}/2m} \left\{ e^{-r_{ij}/m} [1 - \Phi(\sqrt{L}/m - r_{ij}/2\sqrt{L})] - e^{r_{ij}/m} [1 - \Phi(\sqrt{L}/m + r_{ij}/2\sqrt{L})] \right\} \quad (3)$$

where Φ is the error function. U^{MDI} is the momentum dependent interaction (MDI)^[16],

$$U^{MDI} = t_4 \ln^2 [t_5 (\vec{p}_1 - \vec{p}_2)^2 + 1] \frac{\rho}{\rho_0} \quad (4)$$

U^{Pauli} is the Pauli potential^[17–18],

$$U^{Pauli} = V_p \left\{ \frac{\hbar}{p_0 q_0} \right\}^3 \exp\left(-\frac{(\vec{r}_i - \vec{r}_j)^2}{2q_0^2} - \frac{(\vec{p}_i - \vec{p}_j)^2}{2p_0^2}\right) \delta_{p_i p_j} \quad (5)$$

$$\delta_{p_i p_j} = \begin{cases} 1 & \text{for neutron-neutron or proton-proton} \\ 0 & \text{for neutron-proton} \end{cases}$$

U^{sym} is the symmetry potential. In the present paper, three different kinds of U^{sym} have been used^[1],

$$U_1^{sym} = cF_1(u)\delta\tau_z \quad (6)$$

$$U_2^{sym} = cF_2(u)\delta\tau_z + \frac{1}{2}cF_2(u)\delta^2 \quad (7)$$

$$U_3^{sym} = cF_3(u)\delta\tau_z - \frac{1}{4}cF_3(u)\delta^2 \quad (8)$$

with

$$\tau_z = \begin{cases} 1 & \text{for neutron} \\ -1 & \text{for proton} \end{cases}$$

Here c is the strength of the symmetry potential, taking the value of 32MeV. $F_1(u) = u$, $F_2(u) = u^2$ and $F_3(u) = u^{1/2}$, $u \equiv \frac{\rho}{\rho_0}$, δ is the relative neutron excess $\delta = \frac{\rho_n - \rho_p}{\rho_n + \rho_p} = \frac{\rho_n - \rho_p}{\rho}$. ρ and ρ_0 , ρ_n and ρ_p are the nuclear density and its normal value, neutron density and proton density, respectively. The parameters of the interaction potentials are given in table 1.

Table 1. The parameters of the interaction potentials

α	β	γ	t_3	m	t_4	t_5	V_p	p_0	q_0
(MeV)	(MeV)		(MeV)	(fm)	(MeV)	(MeV ⁻²)	(MeV)	(MeV/c)	(fm)
-390.1	320.3	1.14	7.5	0.8	1.57	5×10^{-4}	30	400	5.64

It is worth mentioning that recent studies of collective flow in HIC at intermediate energies have indicated a reduction of the in-medium N-N cross sections^[19–21]. An empirical expression of the in-medium N-N cross section^[21] is used:

$$\sigma_{NN}^{med} = (1 + \alpha \frac{\rho}{\rho_0})\sigma_{NN}^{free} \quad (9)$$

with the parameter $\alpha \approx -0.2$ which has been found to better reproduce the flow data^[19–20]. Here σ_{NN}^{free} is the experimental N-N cross section^[22]. The neutron-proton cross section is about 3 times larger than the proton-proton or neutron-neutron cross section below 300 MeV.

Q_{zz} will be used to describe the nuclear stopping:

$$Q_{ZZ} = \sum_i^A (2P_z(i)^2 - P_x(i)^2 - P_y(i)^2). \quad (10)$$

In order to make the isospin effect on the multifragmentation process in HIC more prominent, comparable study is carried out for two pairs of reversible reaction systems. For each pair of comparable reaction systems the same mass of heavy projectiles and light targets, the same incident energy and the same impact parameter have been used as follows: $^{120}_{48}\text{Cd} + ^{40}_{18}\text{Ar}$ and $^{120}_{54}\text{Xe} + ^{40}_{20}\text{Ca}$ with the neutron-proton ratios 1.42 and 1.16; $^{76}_{30}\text{Zn} + ^{40}_{18}\text{Ar}$ and $^{76}_{36}\text{Kr} + ^{40}_{20}\text{Ca}$ with the neutron-proton ratios 1.42 and 1.07. Hence the differences of N_{imf} and Q_{zz} for each pair of the comparable colliding systems are mainly due to the isospin effect on the process of multifragmentation and dissipation.

By means of the modified isospin-dependent coalescence model^[23], we construct clusters within which the particle relative momentum is smaller than $p_0 = 300\text{MeV}/c$ and the relative distance is smaller than $R_0 = 3.5\text{fm}$. To avoid the nonphysical clusters, the restructured aggregation model^[24] is used until no nonphysical cluster is produced.

3 Results and Discussions

N_{imf} and N_c are calculated event by event with the charge number of IMF from $Z=3$ to 13 for the heavy colliding systems, and $Z=3$ to 8 for the medium mass colliding systems.

3.1 The isospin effect on the process of multifragmentation and dissipation in HIC

Fig.1 shows the time evolution of N_{imf} for the central reactions $^{76}_{30}\text{Zn} + ^{40}_{18}\text{Ar}$ (line 1) and $^{76}_{36}\text{Kr} + ^{40}_{20}\text{Ca}$ (line 2) at $E=80\text{ MeV/nucleon}$ (left panel), and $^{120}_{48}\text{Cd} + ^{40}_{18}\text{Ar}$ (line 1) and $^{120}_{54}\text{Xe} + ^{40}_{20}\text{Ca}$ (line 2) at $E=100\text{ MeV/nucleon}$ (right panel). From Fig.1 one can see that N_{imf} for the two neutron-poor colliding systems $^{120}_{54}\text{Xe} + ^{40}_{20}\text{Ca}$ and $^{76}_{36}\text{Kr} + ^{40}_{20}\text{Ca}$ are larger than those for the neutron-rich systems $^{120}_{48}\text{Cd} + ^{40}_{18}\text{Ar}$ and $^{76}_{30}\text{Zn} + ^{40}_{18}\text{Ar}$. This difference are mainly due to the isospin effect on the multifragmentation because other reaction conditions, except the ratios of neutron to proton, are the same.

As is well known that nuclear reaction mechanism and reaction yields are sensitive to both impact parameter and incident energy. Denoted by the same lines as in Fig.1, Fig.2 depicts the multiplicity of intermediate mass fragments N_{imf} as a function of impact parameter for the two pairs of colliding systems, $^{120}_{48}Cd + ^{40}_{18}Ar$ and $^{120}_{54}Xe + ^{40}_{20}Ca$, $^{76}_{30}Zn + ^{40}_{18}Ar$ and $^{76}_{36}Kr + ^{40}_{20}Ca$. The incident energy E is 100 MeV/nucleon for the heavy systems (left panel), and 80 MeV/nucleon for the medium systems (right panel). As in Fig.1, at small impact parameters, the lines labeled 2 for the neutron-poor colliding systems are always above the corresponding lines labeled 1 for the neutron-rich systems. The difference between them disappears gradually as increasing impact parameter.

Fig.3 shows N_{imf} as a function of beam energy from 15 MeV/nucleon to 200 MeV/nucleon at $b=0$ fm for the above two pairs of colliding systems with the line labels as in Fig.1. The relative locations between the two lines in each panel of the figure are also similar to those in Fig.1, namely, N_{imf} for the two neutron-poor colliding systems $^{120}_{54}Xe + ^{40}_{20}Ca$ and $^{76}_{36}Kr + ^{40}_{20}Ca$ are larger than those for the corresponding neutron-rich systems $^{120}_{48}Cd + ^{40}_{18}Ar$ and $^{76}_{30}Zn + ^{40}_{18}Ar$ for the beam energy above 50 MeV/nucleon. However, as the beam energy decreases to below 50 MeV/nucleon the collision dynamics is governed by both the mean field and the nucleon-nucleon collisions. In this case, the difference between the two lines of the colliding systems in each pair vanishes gradually.

From Figs.1, 2, and 3 we can see that the intermediate mass fragment multiplicity N_{imf} for the neutron-poor colliding system are larger than that of the corresponding neutron-rich system with the same mass projectile on the same mass target and with the same entrance channel conditions except that the ratios of neutron to proton of the colliding systems are different.

The correlation between N_{imf} and N_c for the central collision of the above two pairs of colliding systems with the same beam energies as above is shown in Fig.4. It is seen from the figure that the correlation between N_{imf} and N_c for the two pairs of colliding systems displays a clear isospin effect, i.e., the N_{imf} - N_c correlation for the neutron-poor systems is different from that of the neutron-rich systems. Considering the total yield of N_{imf} (namely the integral area of each curve in the figure), one can

reach the same conclusion as from Fig.1, Fig.2, and Fig.3. This means that the N_{imf} for neutron-poor systems (solid line), on average, is larger than that for the corresponding neutron-rich systems (dash line). The difference comes mainly from the isospin effect on multifragmentation in intermediate energy HIC.

The mechanism of the above fragmentation process can be understood as follows. Experimentally the free neutron-proton cross section is about three times larger than the free neutron-neutron or proton-proton cross section below 300 MeV. The mean N-N cross section is defined as:

$$\langle \sigma \rangle = \frac{N_{np}\sigma_{np} + (N_{nn} + N_{pp})\sigma_{pp}}{N_{np} + N_{pp} + N_{nn}} = \frac{(3N_{np} + N_{nn} + N_{pp})}{N_{np} + N_{nn} + N_{pp}}\sigma_{pp} = (1 + \frac{2N_{np}}{N})\sigma \quad (11)$$

where N_{np} , N_{nn} and N_{pp} are the collision numbers for neutron-proton, neutron-neutron, and proton-proton, respectively, and $N = N_{np} + N_{nn} + N_{pp}$. σ_{np} , σ_{nn} , and σ_{pp} are the free N-N cross sections for neutron-proton, neutron-neutron, and proton-proton, respectively. In general, $\sigma_{nn} = \sigma_{pp} = \sigma$. Because the total collision numbers for two colliding systems with the same mass projectile and the same mass target are the same, and the number of neutron-proton collisions for neutron-poor colliding system is larger than that of the neutron-rich colliding system, the mean total N-N cross section $\langle \sigma \rangle$ of neutron-poor system is thus larger than that of neutron-rich system. Due to the effect of Pauli blocking, the effective collision numbers become smaller. But after considering the Pauli blocking, the above conclusion remains unchanged. Therefore, the neutron-poor system will have more effective N-N collisions and lead to stronger compression-expansion, resulting in a large number of multifragmentation N_{imf} for the neutron-poor system in comparison to the neutron-rich system in the above 50MeV region where the N-N collisions are dominant.

In Fig.5 is plotted the time evolution of the quadrupole of single particle momentum distribution Q_{zz} for the reactions $^{76}Zn + ^{40}Ar$ (dash line) and $^{76}Kr + ^{40}Ca$ (solid line) (bottom panel), $^{120}Cd + ^{40}Ar$ (dash line) and $^{120}Xe + ^{40}Ca$ (solid line)(top panel) at $E=80, 100, 150\text{MeV/nucleon}$ and $b = 0.0\text{fm}$. In the figure, Q_{zz} for the neutron-poor system is always smaller than that of the corresponding neutron-rich system. Smaller Q_{zz} indicates larger dissipation of the initial longitudinal collective motion into the

internal chaotic motion and the subsequent thermalization of the system.

3.2 A good probe and a complementary probe to in-medium N-N cross section

Since the reaction dynamics of HIC is mainly governed by both nuclear EOS and in-medium N-N cross section, to understand the collision dynamics in details, both ingredients should be studied carefully. As is well known that the effects of both ingredients are usually mixed in the dynamics and the main uncertainty of the information about the nuclear EOS extracted from HIC is due to our poor knowledge of the N-N cross section in medium. If one can find an experimental probe which can distinguish the contribution of EOS from that of in-medium N-N cross section, that will be very desirable. In this paper we have found that Q_{zz} may serve as a good probe to in-medium N-N cross section.

In Fig.6 is given Q_{zz} as a function of neutron-proton ratio for seven colliding systems $^{76}Kr + ^{40}Ca$, $^{120}Xe + ^{40}Ca$, $^{64}Ni + ^{40}Ar$, $^{86}Kr + ^{40}Ar$, $^{76}Zn + ^{40}Ar$, $^{85}Ge + ^{40}Ar$, $^{74}Ni + ^{47}Ar$ with the neutron-proton ratios 1.07, 1.16, 1.26, 1.33, 1.42, 1.5 and 1.56 at $E=100\text{MeV/nucleon}$ and $b=0.0\text{ fm}$ for four cases: (1) the symmetry potential U_1^{sym} being employed and in-medium N-N cross section σ_{NN}^{med} being isospin-dependent, namely, $U_1^{sym} + \sigma^{iso}$; (2) U_1^{sym} and N-N cross section σ_{NN}^{med} being isospin-independent, denoted by $U_1^{sym} + \sigma^{noiso}$; (3) U_2^{sym} and σ_{NN}^{med} being isospin-dependent, denoted by $U_2^{sym} + \sigma^{iso}$; (4) U_3^{sym} and σ_{NN}^{med} being isospin-dependent, denoted by $U_3^{sym} + \sigma^{iso}$. In fig.6, lines labeled 1, 2, 3 and 4 correspond to the above four cases.

It is clear to see that Q_{zz} depends strongly on the isospin dependence of in-medium N-N cross section and weakly on the symmetry potential (namely, line 1 is located near lines 3 and 4, but far away from line 2 in Fig.6), though Q_{zz} increases slightly with increasing neutron-proton ratio of asymmetry colliding system. In this case, Q_{zz} is a good probe for extracting information on the isospin dependence of in-medium N-N cross section. We have discussed this in more details in Ref.[12], but it is not clear in Ref.[12] how Q_{zz} depends on the neutron-proton ratio of colliding system. In addition, we shall report a complementary probe for extracting the information on

in-medium N-N cross section: the correlation between the multiplicity of intermediate mass fragments N_{imf} and the total number of charged particles N_c , based on the fact that it is also sensitive to the in-medium N-N cross section and insensitive to the symmetry potential in the chosen energy region. To study the contributions to N_{imf} from different ingredients separately, we consider four cases as the same as in Fig.6.

In Fig.7 is plotted the time evolution of N_{imf} for two different asymmetric colliding systems, $^{76}\text{Zn} + ^{40}\text{Ar}$ at $E = 80\text{MeV/nucleon}$ and $b = 0.0\text{fm}$ (left panel), $^{120}\text{Xe} + ^{40}\text{Ca}$ at $E = 100\text{MeV/nucleon}$ and $b = 0.0\text{fm}$ (right panel). It is noted that lines 1 are always located near lines 3 and 4, but far away from lines 2 with increasing colliding time. This implies that the isospin effect of in-medium N-N cross section on N_{imf} is more important than that of the symmetry potential in the energy region studied here.

As is well known that nuclear reaction products and reaction mechanism sensitively depend on impact parameter. Fig.8 shows the multiplicity of intermediate mass fragments N_{imf} as a function of impact parameter for the four cases as illustrated in Fig.6 for the reactions $^{76}\text{Zn} + ^{40}\text{Ar}$ at $E = 80\text{MeV/nucleon}$ (left panel) and $^{120}\text{Xe} + ^{40}\text{Ca}$ at $E = 100\text{MeV/nucleon}$ (right panel). As in Fig.6, lines 1 in the figures locate near lines 3 and 4, but far away from lines 2 at small impact parameters. This indicates again that the isospin effect of in-medium N-N cross section on N_{imf} is larger in comparison with that of symmetry potential. With increasing impact parameter this isospin effect disappears gradually.

The correlations between N_{imf} and N_c for the four cases are plotted in Fig.9 for the reactions $^{76}\text{Zn} + ^{40}\text{Ar}$ at $E = 80\text{MeV/nucleon}$ (left panel) and $^{120}\text{Xe} + ^{40}\text{Ca}$ at $E = 100\text{MeV/nucleon}$ (right panel). The behaviors of the four kinds of lines in each panel are similar to those in Fig.6, namely, the integral area of the curve 1 is always close to those of the curves 3 and 4, but larger than that of the curve 2. From Fig.7, Fig.8, and Fig.9 one can see that the isospin effect of in-medium N-N cross section on the correlation between N_{imf} and N_c is more important than that of symmetry potential. Here it should be stressed that we have to choose the incident energy for certain asymmetric colliding system carefully to get the above feature, namely, in this

energy region the N-N collisions should be dominant. In this case we may conclude that the correlation between the multiplicity of intermediate mass fragments N_{imf} and the total number of charged particles N_c can be used as a complementary probe to the isospin dependence of the in-medium N-N cross section in HIC.

4 Summary and conclusions

Starting from the simulation of the intermediate energy HIC by using IQMD, the calculated results have shown prominent isospin effects on the process of multifragmentation and dissipation, i.e., the intermediate mass fragment multiplicity N_{imf} for a neutron-poor colliding system is always larger than that of the corresponding neutron-rich system, while the quadrupole of single particle momentum distribution Q_{zz} for a neutron-poor system is smaller than that of the neutron-rich system with the same masses of projectile and target, and the same entrance channel conditions for small impact parameters. We also can see that Q_{zz} increases slight with increasing ratio of neutron to proton in the colliding system.

From the theoretical simulation, it is clear to see that Q_{zz} depends strongly on the isospin dependence of in-medium N-N cross section and weakly on the symmetry potential in the beam energies ranging from about 50 MeV/nucleon to 150MeV/nucleon. And the correlation between N_{imf} and N_c has the same properties as Q_{zz} in the chosen energy region. So we would suggest that Q_{zz} may serve as a good probe and N_{imf} a complementary probe for extracting the information on the isospin dependent N-N cross section in HIC.

Acknowledgment

This work was supported in part by 973 Project Grant No.G2000077400, 100 person Project of the Chinese Academy of Sciences, the National Natural Foundation of China under Grants No. 19775057 and No. 19775020, No. 19847002, No. 19775052 and KJ951-A1-410, and by the Foundation of the Chinese Academy of Sciences

References

- [1] Bao-An Li, Che-Ming Ko et al., *Inter. Jour. Mod. Phys. E*(1998) 147-229.
- [2] M.Colonna, M.DiToro et al., *Phys. Rev. C***57**(1998) 1410-1415.
- [3] B. A. Li. *Phys. Rev. Lett.* 85 (2000)4221-4224.
- [4] Bao-An Li and C. M. Ko, *Nucl. Phys. Nucl. Phys.* **A618**(1997)498.
- [5] Bao-An Li, Che-Ming Ko and Zhong-zhou Ren et al., *Phys. Rev. Lett.* **78**(1997)1644.
- [6] Jian-Ye Liu, Qiang Zhao, Shun-Jin Wang, Wei Zuo, Wen-Jun Guo, *Nucl. Phys. A*, to be published.
- [7] D. R. Bowman, C. M. Mader et al., *Phys. Rev. C***46**(1992)1834.
- [8] M. L. Miller, O. Bjarki et al., *Phys. Rev. Lett.* **82**(1999)1399-1401.
- [9] Yu-Ming Zheng, C. M. Ko, Bao-An Li, Bin Zhang *Phys. Rev. Lett.* **83**(1999)2534.
- [10] R. Pak, W. Benenson, O. Bjarki, J. A. Brown, S. A. Hannuschke, R. A. Lacey, Bao-An Li, A. Nadasen, E. Norbeck, P. Pogodin, D. E. Russ, M. Steiner, N. T. B. Stone, A. M. Vander Molen, G. D. Westfull, L. B. Yang, and S. Y. Yennello, *Phys. Rev. Lett.* **78**(1997) 1022.
- [11] R. Pak, Bao-An Li, W. Benenson, O. Bjarki, J. A. Brown, S. A. Hannuschke, R. A. Lacey, D. J. Magestro, A. Nadasen, E. Norbeck, D. E. Russ, M. Steiner, N. T. B. Stone, A. M. Vander Molen, G. D. Westfall, L. B. Yang, and S. J. Yennello, *Phys. Rev. Lett.* **78**(1997) 1026.
- [12] Jian-Ye Liu, Wen-Jun Guo, Shun-Jin Wang, Wei Zuo, Qiang Zhao. and Yan-Fang Yang, *Phys. Rev. Lett.* **86**(2001)975.
- [13] J. Aichelin, G. Peilert, A. Bohnet, A. Rosenhauer, H. Stocher, and W. Greiner, *Phys. Rev. C***37**(1988) 2451.
- [14] G. Peilert, H. Stocher, and W. Greiner, *Phys. Rev. C***39**(1989)1402.

- [15] P. G. Reinhard, in Computational Nuclear Physics 1, eds. K. Langanke, J. A. Maruhn, and S. E. Koonin, Germany, Springer-Verlag, 1991, P. 28-50.
- [16] J. Aichelin, A. Rosenhauer, G. Peilert, H. Stöcker and W. Greiner, *Phys. Rev. Lett.* **58**(1987) 1926.
- [17] Hang Liu and Jian-Ye Liu, *Z. Phys.* **A345**(1996) 311.
- [18] C. Dorso, S. Duarte, J. Randrup, *Phys. Lett.* **B188**(1987)287.
- [19] M. J. Huang et al., *Phys. Rev. Lett.* **77**(1996)3739.
- [20] G. D. Westfall et al.,*Phys. Rev. Lett.* **71**(1993)1986.
- [21] D. Klakow, G. Welke and W. Bauer, *Phys. Rev.* **C48**(1993)1982.
- [22] K. Chen, Z. Fraenkel et al., *Phys. Rev.* **166**(1968)949.
- [23] G. F. Bertsch and S. D. Gupta, *Phys. Rep.* **160**(1988)1991-233.
- [24] C. Ngo, H. Ngo and S. Leray et al., *Phys. Rep.* 499(1989)148.

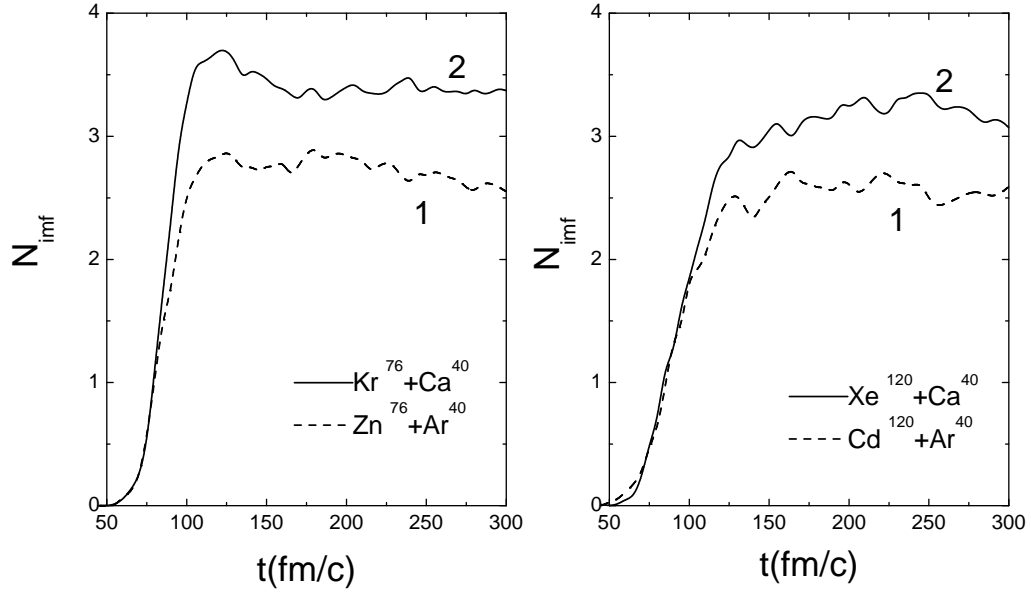


Figure 1: The time evolution of N_{imf} for the central collisions $^{120}\text{Cd} + ^{40}\text{Ar}$ (line 1) and $^{120}\text{Xe} + ^{40}\text{Ca}$ (line 2) at $E = 100$ MeV/nucleon (right panel), $^{76}\text{Zn} + ^{40}\text{Ar}$ (line 1) and $^{76}\text{Kr} + ^{40}\text{Ca}$ (line 2) at $E = 80$ MeV/nucleon (left panel).

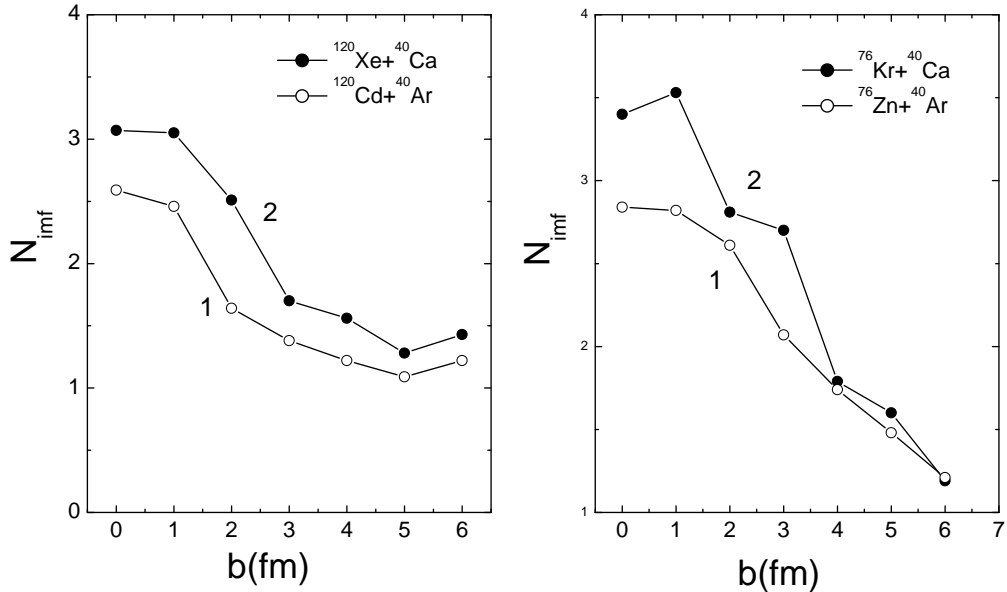


Figure 2: The multiplicity of intermediate mass fragments N_{imf} as a function of impact parameter for the reactions $^{120}\text{Cd} + ^{40}\text{Ar}$ (line 1) and $^{120}\text{Xe} + ^{40}\text{Ca}$ (line 2) at $E = 100$ MeV/nucleon (left panel), and the reactions $^{76}\text{Zn} + ^{40}\text{Ar}$ (line 1) and $^{76}\text{Kr} + ^{40}\text{Ca}$ (line 2) at $E = 80$ MeV/nucleon (right panel).

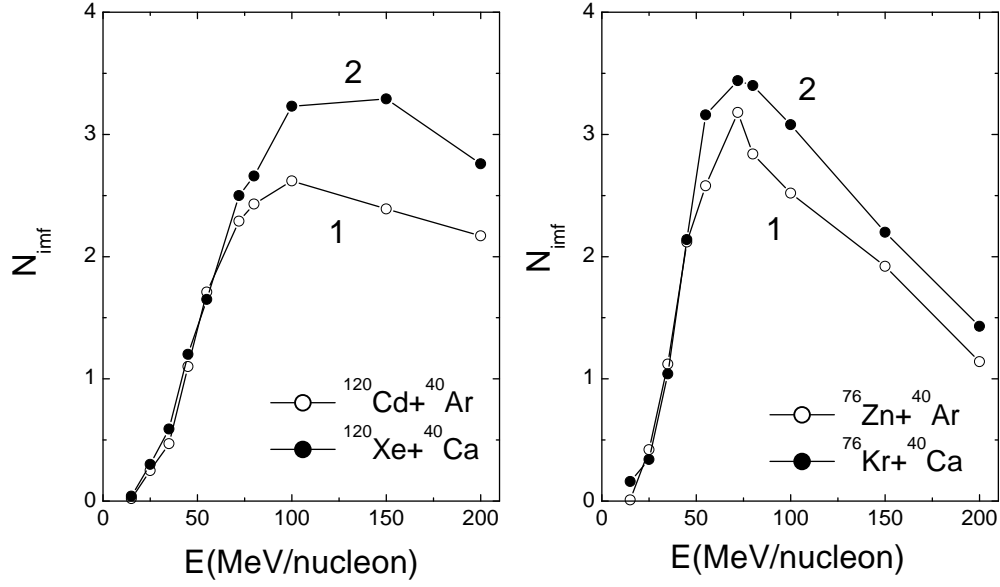


Figure 3: The N_{imf} as a function of incident energies from 15MeV/nucleon to 200MeV/nucleon at $b=0$ fm for the reactions $^{120}\text{Cd} + ^{40}\text{Ar}$ (line 1) and $^{120}\text{Xe} + ^{40}\text{Ca}$ (line 2) at $E = 100$ MeV/nucleon (left panel), and the reactions $^{76}\text{Zn} + ^{40}\text{Ar}$ (line 1) and $^{76}\text{Kr} + ^{40}\text{Ca}$ (line 2) at $E = 80$ MeV/nucleon (right panel).

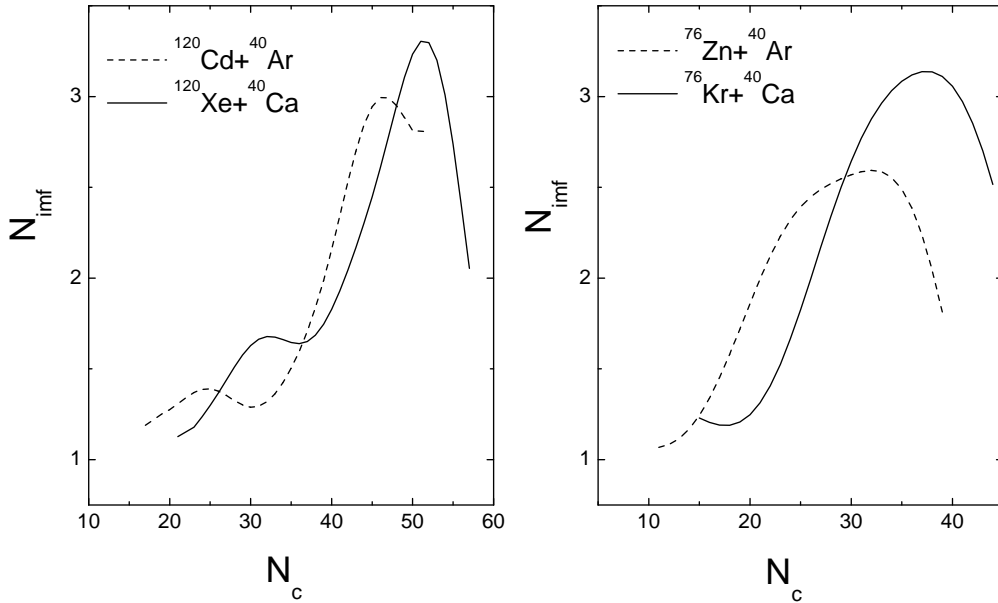


Figure 4: The correlations between N_{imf} and N_c for the reactions $^{120}\text{Cd} + ^{40}\text{Ar}$ (dash line) and $^{120}\text{Xe} + ^{40}\text{Ca}$ (solid line) at $E = 100$ MeV/nucleon (left panel), and the reactions $^{76}\text{Zn} + ^{40}\text{Ar}$ (dash line) and $^{76}\text{Kr} + ^{40}\text{Ca}$ (solid line) at $E = 80$ MeV/nucleon (right panel).

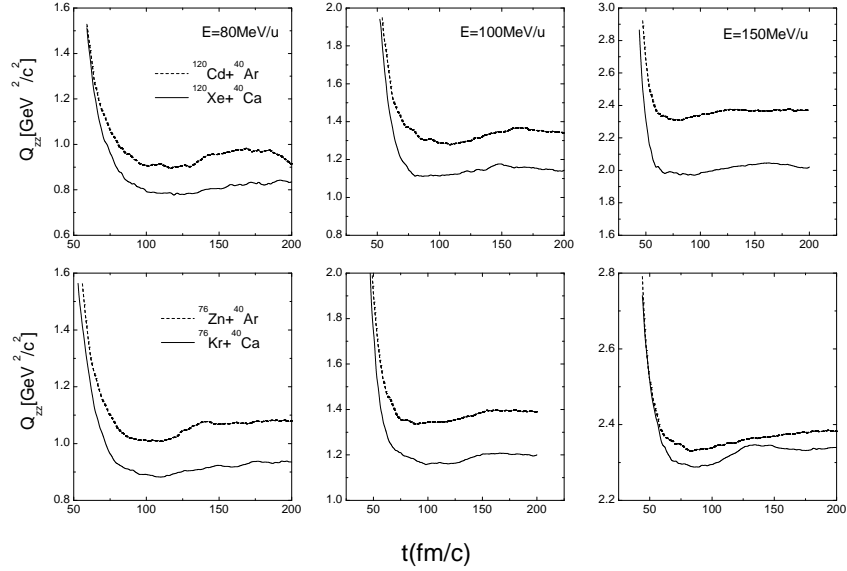


Figure 5: The time evolution of the quadrupole of single particle momentum distribution Q_{zz} for the reactions $^{76}\text{Zn} + ^{40}\text{Ar}$ (dash line) and $^{76}\text{Kr} + ^{40}\text{Ca}$ (solid line) (bottom panel), and the reactions $^{120}\text{Cd} + ^{40}\text{Ar}$ (dash line) and $^{120}\text{Xe} + ^{40}\text{Ca}$ (solid line) (top panel) at $E=80, 100$ and 150MeV/nucleon and $b = 0.0\text{fm}$.

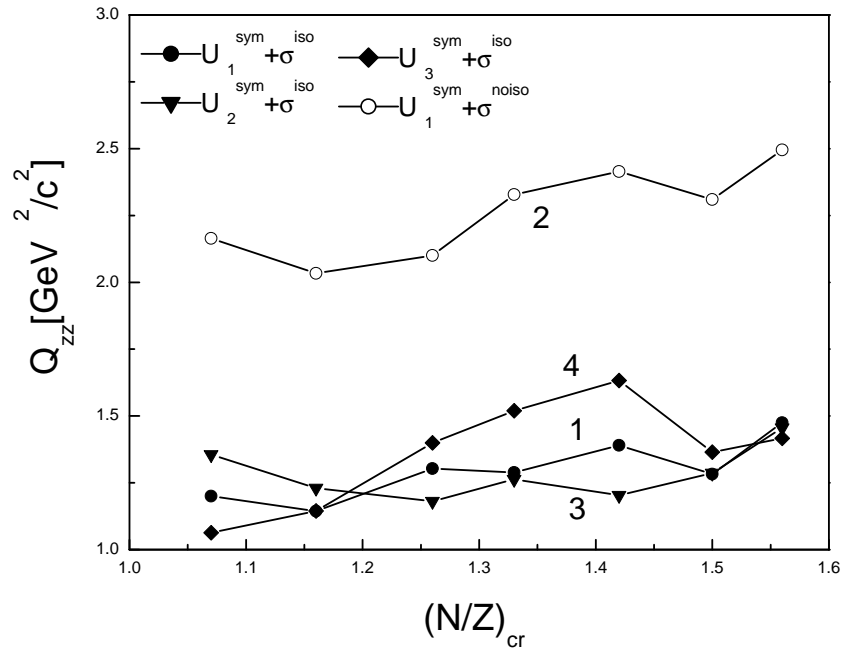


Figure 6: The quadrupole of single particle momentum distribution Q_{zz} as a function of the neutron-proton ratio for seven colliding systems $^{76}\text{Kr} + ^{40}\text{Ca}$, $^{120}\text{Xe} + ^{40}\text{Ca}$, $^{64}\text{Ni} + ^{40}\text{Ar}$, $^{86}\text{Kr} + ^{40}\text{Ar}$, $^{76}\text{Zn} + ^{40}\text{Ar}$, $^{85}\text{Ge} + ^{40}\text{Ar}$, and $^{74}\text{Ni} + ^{47}\text{Ar}$ at $E = 100\text{MeV/nucleon}$ and $b = 0.0\text{fm}$ for the four cases (see text).

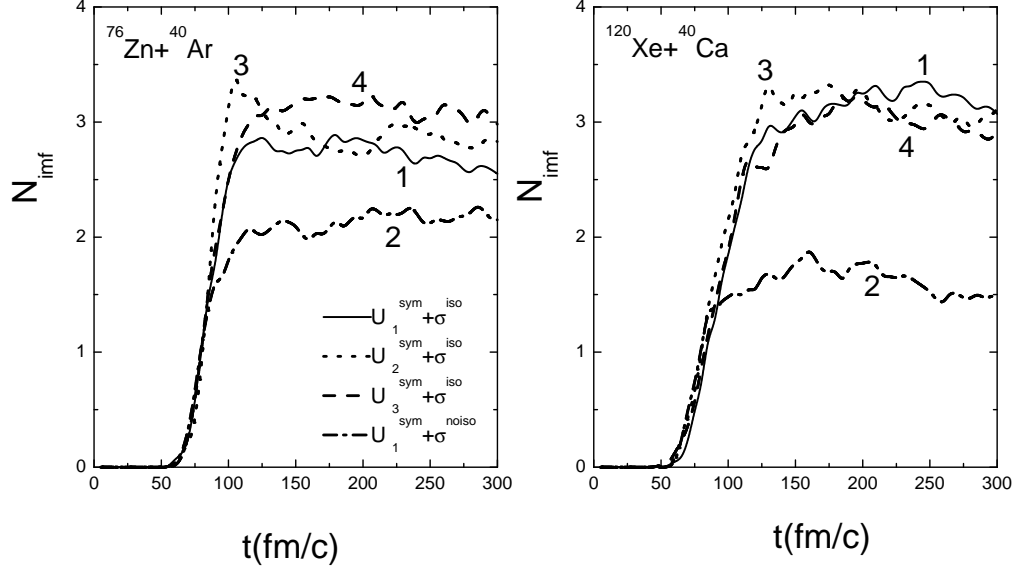


Figure 7: The time evolution of N_{imf} for the reactions $^{76}\text{Zr} + ^{40}\text{Ar}$ at $E = 80$ MeV/nucleon and $b = 0.0$ fm (left panel), $^{120}\text{Xe} + ^{40}\text{Ca}$ at $E = 100$ MeV/nucleon and $b = 0.0$ fm (right panel). Lines 1, 2, 3, and 4 correspond to the four cases as in Fig.6.

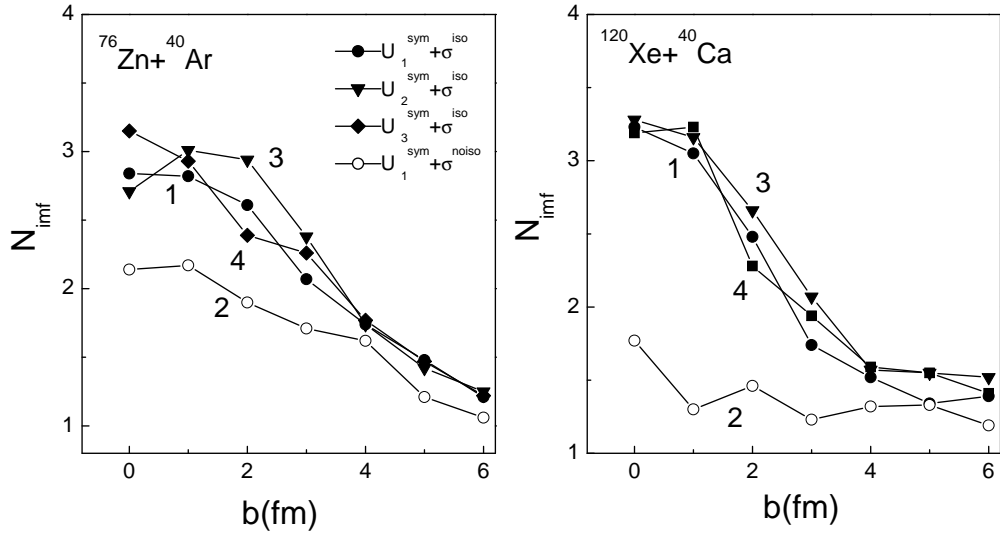


Figure 8: The multiplicity of intermediate mass fragments N_{imf} as a function of impact parameter for the reactions $^{76}\text{Zn} + ^{40}\text{Ar}$ at $E = 80$ MeV/nucleon (left panel) and $^{120}\text{Xe} + ^{40}\text{Ca}$ at $E = 100$ MeV/nucleon (right panel) in the four cases as in Fig.6.

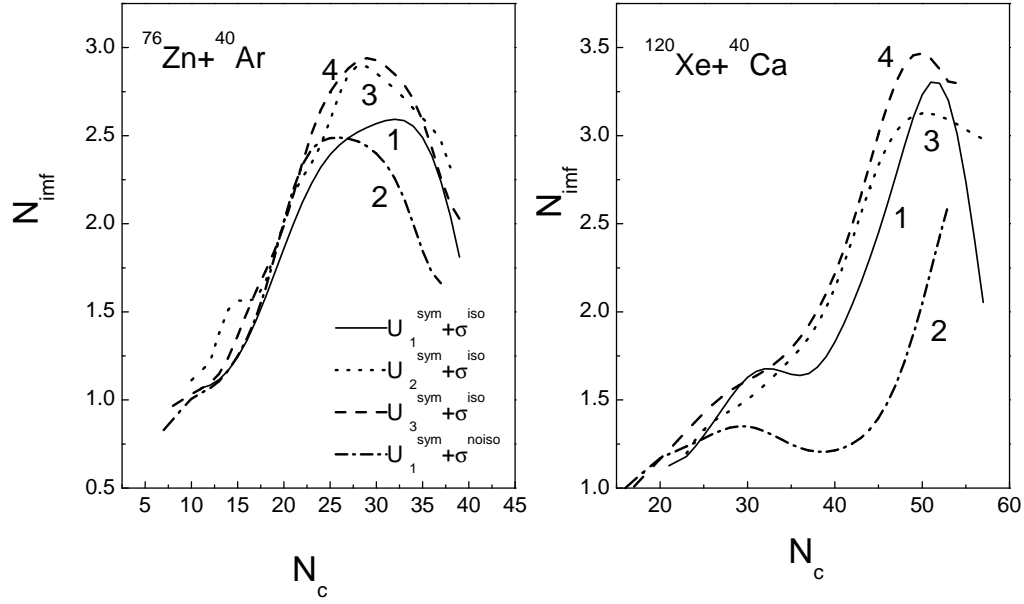


Figure 9: The correlations between N_{inf} and N_c for the reactions $^{76}\text{Zn} + ^{40}\text{Ar}$ at $E = 80\text{MeV/nucleon}$ (left panel) and $^{120}\text{Xe} + ^{40}\text{Ca}$ at $E = 100\text{MeV/nucleon}$ (right panel) for the four cases as in Fig.6.